 CMES, vol.89, no.3, pp.189-220, 2012

High-order Alternating Direction Implicit Method Based on Compact Integrated-RBF Approximations for Unsteady/Steady Convection-Diffusion Equations

N. Thai-Quang[1], N. Mai-Duy[1], C.-D Tran[1] and T. Tran-Cong[1]

Abstract: In this paper, the alternating direction implicit (ADI) method reported in [You (2006)] for the convection-diffusion equation is implemented in the context of compact integrated radial basis function (CIRBF) approximations. The CIRBF approximations are constructed over 3-point stencils, where extra information is incorporated via two forms: only nodal second-order derivative values (Scheme 1), and both nodal first- and second-order derivative values (Scheme 2). The resultant algebraic systems are sparse, especially for Scheme 2 (tridiagonal matrices). Several steady and non-steady problems are considered to verify the present schemes and to compare their accuracy with some other ADI schemes. Numerical results show that highly accurate results are obtained with the proposed methods.

Keywords: compact integrated-RBF stencils, high-order approximations, alternating direction implicit (ADI), convection-diffusion equation.

1 Introduction

In this paper, we consider a two-dimensional (2D) unsteady convection-diffusion equation for a variable u

$$\frac{\partial u}{\partial t}+c_x\frac{\partial u}{\partial x}+c_y\frac{\partial u}{\partial y}=d_x\frac{\partial^2 u}{\partial x^2}+d_y\frac{\partial^2 u}{\partial y^2}+f_b, \quad (x,y,t)\in\Omega\times[0,T], \tag{1}$$

subject to the initial condition

$$u(x,y,0)=u_0(x,y), \quad (x,y)\in\Omega, \tag{2}$$

and Dirichlet boundary condition

$$u(x,y,t)=u_\Gamma(x,y,t), \quad (x,y)\in\Gamma, \tag{3}$$

[1] Computational Engineering and Science Research Centre, Faculty of Engineering and Surveying, The University of Southern Queensland, Toowoomba, Queensland 4350, Australia.

where Ω is a two-dimensional rectangular domain; Γ the boundary of Ω; $[0,T]$ the time interval; f_b the driving function; and u_0, u_Γ some given functions. In equation (1), c_x and c_y are the convective velocities, and d_x and d_y are the positive diffusion coefficients.

For the steady-state case, equation (1) reduces to

$$c_x \frac{\partial u}{\partial x} + c_y \frac{\partial u}{\partial y} = d_x \frac{\partial^2 u}{\partial x^2} + d_y \frac{\partial^2 u}{\partial y^2} + f_b. \tag{4}$$

Equations (1) and (4) are known as a simplified version of the Navier-Stokes equation. They are widely used in computational fluid dynamics (CFD) and physical sciences to describe the transport of mass, momentum, vorticity, heat and energy, the modeling of semiconductors, *etc*. For example, by means of (1), one can describe the heat transfer in a draining film [Isenberg and Gutfinger (1972)], water transfer in soils [Parlange (1980)] and the chemical separation processes [Dehghan (2004)].

It is desirable to have accurate and stable methods for solving the convection-diffusion equation. The upwind and central finite differences are among popular discretisation schemes for the approximation of spatial derivative terms because they are simple and easy to implement. These finite-difference schemes generally yield good results on sufficiently fine meshes. However, poor results may be obtained if the mesh used is relatively coarse. To improve the accuracy order, larger stencils can be used. The drawback of this approach is that the bandwidth of their coefficient matrices is increased, and thus it is time-consuming to solve such systems either by using direct solvers, *e.g.* Gaussian elimination and LU decomposition technique, or iterative methods, *e.g.* a generalized minimal residual algorithm (GMRES) and biconjugate gradient stabilised method (BICGSTAB). This leads to the development of compact finite difference methods, where small matrix bandwidth and high-order accuracy can be achieved together [Noye and Tan (1989); Kalita, Dalal, and Dass (2002); Kalita and Chhabra (2006)].

The ADI methods are highly efficient procedures for solving parabolic and hyperbolic problems [Thomas (1995)]. As shown in [Thomas (1995)], the efficiency of ADI methods is based on reducing problems in several space variables to a number of one-dimensional problems. The standard PR-ADI method [Peaceman and H. H. Rachford (1955)] has been popular because of its computational cost-effectiveness. However, due to its low-order accuracy, the method often produces significant dissipation and phase errors [Karaa and Zhang (2004)]. To enhance spatial accuracy, Karaa and Zhang (2004) has developed a high-order compact ADI (HOC-ADI) scheme, which possesses fourth-order accuracy and still retains the tridiagonal algorithm of the standard PR-ADI. For solving the convection-

dominated diffusion (CDD) equation (*i.e.* high Peclet numbers), HOC-based schemes may suffer from excessive numerical dissipation [You (2006); Ma, Sun, Haake, Churchill, and Ho (2012)]. A high-order ADI method proposed in [You (2006)] was designed to overcome this problem, where its factorisation involves 4 terms and spatial derivatives are approximated using the Pad' algorithm.

In this paper, we implement the ADI method proposed in [You (2006)] in the context of CIRBF approximations for the convection-diffusion equation. Two compact 3-point schemes, namely ADI-CIRBF-1 and ADI-CIRBF-2, for the spatial discretisation are proposed. Scheme 1 incorporates nodal values of the second-order derivatives into the approximations, while Scheme 2 includes not only nodal second-order derivative values but also nodal first-derivative values. The resultant algebraic systems are sparse, especially for Scheme 2 (tridiagonal matrices). The performances of the two present schemes are investigated numerically through the solution of several analytic test problems governed by the unsteady and steady 2D convection-diffusion equations. Results obtained are also compared with those obtained by the standard PR-ADI scheme and some other high-order compact ADI schemes. The remainder of the paper is organised as follows. Section 2 gives a brief review of some ADI methods. Section 3 describes the two proposed schemes. In section 4, numerical results are presented and compared with some published solutions. Section 5 concludes the paper.

2 A brief review of ADI methods

2.1 The Peaceman-Rachford method

The PR-ADI method splits equation (1) into two

$$\frac{u^{n-1/2}-u^{n-1}}{\Delta t/2}+c_x\frac{\partial u^{n-1/2}}{\partial x}+c_y\frac{\partial u^{n-1}}{\partial y}=d_x\frac{\partial^2 u^{n-1/2}}{\partial x^2}+d_y\frac{\partial^2 u^{n-1}}{\partial y^2}+f_b^{n-1/2}, \quad (5)$$

$$\frac{u^{n}-u^{n-1/2}}{\Delta t/2}+c_x\frac{\partial u^{n-1/2}}{\partial x}+c_y\frac{\partial u^{n}}{\partial y}=d_x\frac{\partial^2 u^{n-1/2}}{\partial x^2}+d_y\frac{\partial^2 u^{n}}{\partial y^2}+f_b^{n-1/2}, \quad (6)$$

where the derivatives with respect to x and y are treated implicitly in the first and second equations, respectively. The PR-ADI method often leads to significant dissipation and phase errors due to its low-order accuracy in the spatial discretisation.

2.2 The Douglas-Rachford method

The Douglas-Rachford method [Douglas and Rachford (1956)] is a variant of the Peaceman-Rachford method. Applying this method to (1), one obtains

$$\frac{u^{*,n}-u^{n-1}}{\Delta t}+c_x\frac{\partial u^{*,n}}{\partial x}+c_y\frac{\partial u^{n-1}}{\partial y}=d_x\frac{\partial^2 u^{*,n}}{\partial x^2}+d_y\frac{\partial^2 u^{n-1}}{\partial y^2}+f_b^{n}, \quad (7)$$

$$\frac{u^n - u^{n-1}}{\Delta t} + c_x \frac{\partial u^{*,n}}{\partial x} + c_y \frac{\partial u^n}{\partial y} = d_x \frac{\partial^2 u^{*,n}}{\partial x^2} + d_y \frac{\partial^2 u^n}{\partial y^2} + f_b^n, \tag{8}$$

Unlike the Peaceman-Rachford method, this scheme is very easy to generalise to operator decompositions involving more than two operators [Glowinski, Ciarlet, and Lions (2003)]. However, it still retains the drawbacks of the standard Peaceman-Rachford method.

2.3 Karaa's method

This method factorises equation (1) as

$$\left(L_x + \frac{\Delta t}{2} A_x\right)\left(L_y + \frac{\Delta t}{2} A_y\right) u^n = \left(L_x - \frac{\Delta t}{2} A_x\right)\left(L_y - \frac{\Delta t}{2} A_y\right) u^{n-1}, \tag{9}$$

where

$$L_x = 1 + \frac{\Delta x^2}{12}\left(\delta_x^2 - \frac{c_x}{d_x}\delta_x\right), \quad A_x = -\left(d_x + \frac{c_x^2 \Delta x^2}{12 d_x}\right)\delta_x^2 + c_x \delta_x, \tag{10}$$

$$L_y = 1 + \frac{\Delta y^2}{12}\left(\delta_y^2 - \frac{c_y}{d_y}\delta_y\right), \quad A_y = -\left(d_y + \frac{c_y^2 \Delta y^2}{12 d_y}\right)\delta_y^2 + c_y \delta_y, \tag{11}$$

δ_η and δ_η^2 are the first- and second-order central difference operators for η-direction; and Δx and Δy the mesh size.

Introducing an intermediate variable u^*, equation (9) can be solved by the following two steps

$$\left(L_x + \frac{\Delta t}{2} A_x\right) u^* = \left(L_x - \frac{\Delta t}{2} A_x\right)\left(L_y - \frac{\Delta t}{2} A_y\right) u^{n-1}, \tag{12}$$

$$\left(L_y + \frac{\Delta t}{2} A_y\right) u^n = u^*. \tag{13}$$

2.4 You's method

You (2006) proposed the following factorisation to equation (1)

$$\begin{aligned}\left(1 + \frac{\Delta t}{2} c_x \frac{\partial}{\partial x}\right)\left(1 - \frac{\Delta t}{2} d_x \frac{\partial^2}{\partial x^2}\right)\left(1 + \frac{\Delta t}{2} c_y \frac{\partial}{\partial y}\right)\left(1 - \frac{\Delta t}{2} d_y \frac{\partial^2}{\partial y^2}\right) u^n \\ = \left(1 - \frac{\Delta t}{2} c_x \frac{\partial}{\partial x}\right)\left(1 + \frac{\Delta t}{2} d_x \frac{\partial^2}{\partial x^2}\right)\left(1 - \frac{\Delta t}{2} c_y \frac{\partial}{\partial y}\right)\left(1 + \frac{\Delta t}{2} d_y \frac{\partial^2}{\partial y^2}\right) u^{n-1} \\ + \Delta t f_b^{n-1/2}.\end{aligned} \tag{14}$$

In the matrix-vector notation, equation (14) becomes

$$L_x^{-1}T_x^+L_{xx}^{-1}T_{xx}^-L_y^{-1}T_y^+L_{yy}^{-1}T_{yy}^-u^n = L_x^{-1}T_x^-L_{xx}^{-1}T_{xx}^+L_y^{-1}T_y^-L_{yy}^{-1}T_{yy}^+u^{n-1}, \tag{15}$$

where

$$T_x^{\pm} = \left(L_x \pm \frac{\Delta t}{2}c_xA_x\right), \qquad T_{xx}^{\pm} = \left(L_{xx} \pm \frac{\Delta t}{2}d_xB_{xx}\right), \tag{16}$$
$$T_y^{\pm} = \left(L_y \pm \frac{\Delta t}{2}c_yA_y\right), \qquad T_{yy}^{\pm} = \left(L_{yy} \pm \frac{\Delta t}{2}d_yB_{yy}\right),$$

L_x, L_{xx}, A_x, B_{xx}, L_y, L_{yy}, A_y and B_{yy} are coefficient matrices derived from the standard fourth-order Pad' schemes.

The equation (15) can be solved by the following two steps

$$L_x^{-1}T_x^+L_{xx}^{-1}T_{xx}^-u^* = L_x^{-1}T_x^-L_{xx}^{-1}T_{xx}^+L_y^{-1}T_y^-L_{yy}^{-1}T_{yy}^+u^{n-1}, \tag{17}$$
$$L_y^{-1}T_y^+L_{yy}^{-1}T_{yy}^-u^n = u^*. \tag{18}$$

The last two ADI methods (section 2.3 and 2.4) are preferable to the first two methods (section 2.1 and 2.2) in solving the convection-dominated diffusion (CDD) equation.

3 Proposed schemes

We propose two high-order numerical schemes, which are based on compact integrated-RBF approximations, for the spatial discretisation, and incorporated them into the ADI framework proposed in [You (2006)].

3.1 Spatial discretisation

Consider a two-dimensional domain Ω, where a uniform Cartesian grid is used to represent the domain, and the nodes are indexed in the x-direction by the subscript i ($i \in \{1,2,\ldots,n_x\}$) and in y-direction by j ($j \in \{1,2,\ldots,n_y\}$). Let N be the total number of nodes (*i.e.* $N = n_x \times n_y$) and N_{ip} be the number of interior nodes (*i.e.* $N_{ip} = (n_x-2)\times(n_y-2)$).

At an interior grid point $\widehat{x}_{i,j} = (x_{i,j}, y_{i,j})^T$ ($i \in \{2,3,\ldots,n_x-1\}$ and $j \in \{2,3,\ldots,n_y-1\}$), the associated stencils to be considered here are (i) two local stencils: $[x_{i-1,j}, x_{i,j}, x_{i+1,j}]$ in the x-direction and $[y_{i,j-1}, y_{i,j}, y_{i,j+1}]$ in the y-direction, and (ii) two global stencils: $[x_{1,j}, x_{2,j}, \ldots, x_{n_x,j}]$ ($x_{1,j}$ and $x_{n_x,j}$ are the two boundary nodes) in the x-direction and $[y_{i,1}, y_{i,2}, \ldots, y_{i,n_y}]$ ($y_{i,1}$ and y_{i,n_y} the two boundary nodes) in the y-direction. Hereafter, for brevity, we use η to denote x and y, and thus to have a generic local

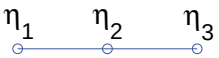

Figure 1: Compact 3-point 1D-IRBF stencil.

Figure 2: Global 1D-IRBF stencil.

stencil $[\eta_1, \eta_2, \eta_3]$ ($\eta_1 < \eta_2 < \eta_3,\ \eta_2 \equiv \eta_{i,j}$) (Figure 1) and a generic global stencil $\left[\eta_1, \eta_2, \ldots, \eta_{n_\eta}\right]$ (Figure 2).

The integral approach starts with the decomposition of second-order derivatives of u into RBFs

$$\frac{d^2u(\eta)}{d\eta^2} = \sum_{i=1}^{m} w_i G_i(\eta), \tag{19}$$

where $\{G_i(\eta)\}_{i=1}^m$ is the set of RBFs; and $\{w_i\}_{i=1}^m$ the set of weights/coefficients to be found. Approximate representations for the first-order derivative and the function itself are then obtained through integration

$$\frac{du(\eta)}{d\eta} = \sum_{i=1}^{m} w_i H_i(\eta) + c_1, \tag{20}$$

$$u(\eta) = \sum_{i=1}^{m} w_i \overline{H}_i(\eta) + c_1\eta + c_2, \tag{21}$$

where $H_i(\eta) = \int G_i(\eta)d\eta$; $\overline{H}_i(\eta) = \int H_i(\eta)d\eta$; and c_1 and c_2 are the constants of integration.

Below are two proposed schemes whose constructions are based on (19)-(21). The difference between the two lies in (i) types of nodal derivatives used in their compact forms (*i.e.* second-order derivatives only for the first proposed scheme, and both first- and second-order derivatives for the second proposed scheme); and (ii) approximations for the boundary derivative values (*i.e.* global approximations for the first scheme and compact local approximations for the second scheme). The value of m is taken to be 3 for local stencils, and n_x or n_y for global stencils.

3.1.1 CIRBF-1

Over a 3-point stencil associated with an interior node, we establish the relation between the physical space and the RBF space as follows

$$\begin{pmatrix} u_1 \\ u_2 \\ u_3 \\ \frac{d^2u_1}{d\eta^2} \\ \frac{d^2u_3}{d\eta^2} \end{pmatrix} = \underbrace{\begin{pmatrix} \overline{\mathscr{H}} \\ \mathscr{G} \end{pmatrix}}_{\mathscr{C}_1} \begin{pmatrix} w_1 \\ w_2 \\ w_3 \\ c_1 \\ c_2 \end{pmatrix}, \tag{22}$$

where $u_i = u(\eta_i)$ $(i \in \{1,2,3\})$; $\frac{d^2u_i}{d\eta^2} = \frac{d^2u}{d\eta^2}(\eta_i)$ $(i \in \{1,3\})$; $\mathscr{C}_1$ is the conversion matrix; and $\overline{\mathscr{H}}, \mathscr{G}$ are matrices defined as

$$\overline{\mathscr{H}} = \begin{bmatrix} \overline{H}_1(\eta_1) & \overline{H}_2(\eta_1) & \overline{H}_3(\eta_1) & \eta_1 & 1 \\ \overline{H}_1(\eta_2) & \overline{H}_2(\eta_2) & \overline{H}_3(\eta_2) & \eta_2 & 1 \\ \overline{H}_1(\eta_3) & \overline{H}_2(\eta_3) & \overline{H}_3(\eta_3) & \eta_3 & 1 \end{bmatrix}, \tag{23}$$

$$\mathscr{G} = \begin{bmatrix} G_1(\eta_1) & G_2(\eta_1) & G_3(\eta_1) & 0 & 0 \\ G_1(\eta_3) & G_2(\eta_3) & G_3(\eta_3) & 0 & 0 \end{bmatrix}. \tag{24}$$

Solving (22) yields

$$\begin{pmatrix} w_1 \\ w_2 \\ w_3 \\ c_1 \\ c_2 \end{pmatrix} = \mathscr{C}_1^{-1} \begin{pmatrix} u_1 \\ u_2 \\ u_3 \\ \frac{d^2u_1}{d\eta^2} \\ \frac{d^2u_3}{d\eta^2} \end{pmatrix}, \tag{25}$$

which maps the vector of nodal values of the function and of its second-order derivative to the vector of RBF coefficients including the two integration constants.

First-order derivative compact approximations:

Approximate expressions for the first-order derivatives in the physical space are obtained by substituting (25) into (20)

$$\frac{du(\eta)}{d\eta} = \begin{bmatrix} H_1(\eta) & H_2(\eta) & H_3(\eta) & 1 & 0 \end{bmatrix} \mathscr{C}_1^{-1} \begin{pmatrix} \widehat{u} \\ \widehat{\frac{d^2u}{d\eta^2}} \end{pmatrix}, \tag{26}$$

where $\eta_1 \le \eta \le \eta_3$; $\widehat{u} = (u_1, u_2, u_3)^T$ and $\widehat{\frac{d^2u}{d\eta^2}} = (\frac{d^2u_1}{d\eta^2}, \frac{d^2u_3}{d\eta^2})^T$.

(26) can be rewritten as

$$\frac{du(\eta)}{d\eta} = \sum_{i=1}^{3} \frac{d\varphi_i(\eta)}{d\eta} u_i + \frac{d\varphi_4(\eta)}{d\eta} \frac{d^2u_1}{d\eta^2} + \frac{d\varphi_5(\eta)}{d\eta} \frac{d^2u_3}{d\eta^2}, \tag{27}$$

where $\{\varphi_i(\eta)\}_{i=1}^{5}$ is the set of IRBFs in the physical space.
At the current time level n, equation (27) is treated in an implicit manner as

$$\frac{du^n(\eta)}{d\eta} = \sum_{i=1}^{3} \frac{d\varphi_i(\eta)}{d\eta} u_i^n + \frac{d\varphi_4(\eta)}{d\eta} \frac{d^2u_1^n}{d\eta^2} + \frac{d\varphi_5(\eta)}{d\eta} \frac{d^2u_3^n}{d\eta^2}, \tag{28}$$

where the nodal second-order derivative values are also considered as unknowns. Collocating (28) at $\eta = \eta_2$ results in

$$\frac{du_2^n}{d\eta} = \frac{d\varphi_1(\eta_2)}{d\eta} u_1^n + \frac{d\varphi_2(\eta_2)}{d\eta} u_2^n + \frac{d\varphi_3(\eta_2)}{d\eta} u_3^n + \frac{d\varphi_4(\eta_2)}{d\eta} \frac{d^2u_1^n}{d\eta^2} + \frac{d\varphi_5(\eta_2)}{d\eta} \frac{d^2u_3^n}{d\eta^2}, \tag{29}$$

or in matrix-vector form

$$\begin{bmatrix} 0 & 1 & 0 \end{bmatrix} \begin{bmatrix} \frac{du_1^n}{d\eta} \\ \frac{du_2^n}{d\eta} \\ \frac{du_3^n}{d\eta} \end{bmatrix} =$$

$$\begin{bmatrix} \frac{d\varphi_1(\eta_2)}{d\eta} & \frac{d\varphi_2(\eta_2)}{d\eta} & \frac{d\varphi_3(\eta_2)}{d\eta} \end{bmatrix} \begin{bmatrix} u_1^n \\ u_2^n \\ u_3^n \end{bmatrix} + \begin{bmatrix} \frac{d\varphi_4(\eta_2)}{d\eta} & 0 & \frac{d\varphi_5(\eta_2)}{d\eta} \end{bmatrix} \begin{bmatrix} \frac{d^2u_1^n}{d\eta^2} \\ \frac{d^2u_2^n}{d\eta^2} \\ \frac{d^2u_3^n}{d\eta^2} \end{bmatrix}. \tag{30}$$

At the boundary nodes, nodal values of the first-order derivatives are approximated using the global 1D-IRBF approach [Mai-Duy and Tran-Cong (2008)]

$$\begin{pmatrix} \frac{du_1^n}{d\eta} \\ \frac{du_{n_\eta}^n}{d\eta} \end{pmatrix} =$$

$$\begin{bmatrix} H_1(\eta_1) & H_1(\eta_{n_\eta}) \\ \vdots & \vdots \\ H_{n_\eta}(\eta_1) & H_{n_\eta}(\eta_{n_\eta}) \\ 1 & 1 \\ 0 & 0 \end{bmatrix}^T \begin{bmatrix} \overline{H}_1(\eta_1) & \cdots & \overline{H}_{n_\eta}(\eta_1) & \eta_1 & 1 \\ \overline{H}_1(\eta_2) & \cdots & \overline{H}_{n_\eta}(\eta_2) & \eta_2 & 1 \\ \vdots & \ddots & \vdots & \vdots & \vdots \\ \overline{H}_1(\eta_{n_\eta}) & \cdots & \overline{H}_{n_\eta}(\eta_{n_\eta}) & \eta_{n_\eta} & 1 \end{bmatrix}^{-1} \begin{pmatrix} u_1^n \\ u_2^n \\ \vdots \\ u_{n_\eta}^n \end{pmatrix}, \tag{31}$$

where $u_i = u(\eta_i)$ $(i \in \{1,2,\ldots,n_\eta\})$; and $\frac{du_i}{d\eta} = \frac{du}{d\eta}(\eta_i)$ $(i \in \{1,n_\eta\})$.
The IRBF system on a grid line for the first-order derivative of u is obtained by letting the interior node taking value from 2 to $(n_\eta - 1)$ in (30) and making use of (31)

$$\mathscr{L}_\eta \widehat{u}^n_\eta = \mathscr{A}_\eta \widehat{u}^n + \mathscr{A}_{\eta\eta} \widehat{u}^n_{\eta\eta}, \tag{32}$$

where $\mathscr{L}_\eta$, $\mathscr{A}_\eta$ and $\mathscr{A}_{\eta\eta}$ are $n_\eta \times n_\eta$ matrices, and

$$\widehat{u}^n = \left[u^n_1, u^n_2, \ldots, u^n_{n_\eta}\right]^T, \tag{33}$$

$$\widehat{u}^n_\eta = \left[\frac{du^n_1}{d\eta}, \frac{du^n_2}{d\eta}, \ldots, \frac{du^n_{n_\eta}}{d\eta}\right]^T, \tag{34}$$

$$\widehat{u}^n_{\eta\eta} = \left[\frac{d^2u^n_1}{d\eta^2}, \frac{d^2u^n_2}{d\eta^2}, \ldots, \frac{d^2u^n_{n_\eta}}{d\eta^2}\right]^T. \tag{35}$$

Second-order derivative compact approximations:

Approximate expressions for the second-order derivatives in the physical space are obtained by substituting (25) into (19)

$$\frac{d^2u(\eta)}{d\eta^2} = \left[\begin{array}{ccccc} G_1(\eta) & G_2(\eta) & G_3(\eta) & 0 & 0 \end{array}\right] \mathscr{C}_1^{-1} \left(\begin{array}{c} \widehat{u} \\ \widehat{\frac{d^2u}{d\eta^2}} \end{array}\right), \tag{36}$$

or

$$\frac{d^2u^n(\eta)}{d\eta^2} = \sum_{i=1}^{3} \frac{d^2\varphi_i(\eta)}{d\eta^2} u^n_i + \frac{d^2\varphi_4(\eta)}{d\eta^2}\frac{d^2u^n_1}{d\eta^2} + \frac{d^2\varphi_5(\eta)}{d\eta^2}\frac{d^2u^n_3}{d\eta^2}. \tag{37}$$

Collocating (37) at $\eta = \eta_2$ leads to

$$-\frac{d^2\varphi_4(\eta_2)}{d\eta^2}\frac{d^2u^n_1}{d\eta^2} + \frac{d^2u^n_2}{d\eta^2} - \frac{d^2\varphi_5(\eta_2)}{d\eta^2}\frac{d^2u^n_3}{d\eta^2} = \frac{d^2\varphi_1(\eta_2)}{d\eta^2}u^n_1 + \frac{d^2\varphi_2(\eta_2)}{d\eta^2}u^n_2 + \frac{d^2\varphi_3(\eta_2)}{d\eta^2}u^n_3, \tag{38}$$

or in matrix-vector form

$$\left[\begin{array}{ccc} -\frac{d^2\varphi_4(\eta_2)}{d\eta^2} & 1 & -\frac{d^2\varphi_5(\eta_2)}{d\eta^2} \end{array}\right] \left[\begin{array}{c} \frac{d^2u^n_1}{d\eta^2} \\ \frac{d^2u^n_2}{d\eta^2} \\ \frac{d^2u^n_3}{d\eta^2} \end{array}\right] = \left[\begin{array}{ccc} \frac{d^2\varphi_1(\eta_2)}{d\eta^2} & \frac{d^2\varphi_2(\eta_2)}{d\eta^2} & \frac{d^2\varphi_3(\eta_2)}{d\eta^2} \end{array}\right] \left[\begin{array}{c} u^n_1 \\ u^n_2 \\ u^n_3 \end{array}\right]. \tag{39}$$

At the boundary nodes, nodal values of the second-order derivatives are approximated as [Mai-Duy and Tran-Cong (2008); Thai-Quang, Le-Cao, Mai-Duy, and Tran-Cong (2012)]

$$\begin{pmatrix} \frac{d^2u_1^n}{d\eta^2} \\ \frac{d^2u_{n_\eta}^n}{d\eta^2} \end{pmatrix} = \begin{bmatrix} G_1(\eta_1) & G_1(\eta_{n_\eta}) \\ \vdots & \vdots \\ G_{n_\eta}(\eta_1) & G_{n_\eta}(\eta_{n_\eta}) \\ 0 & 0 \\ 0 & 0 \end{bmatrix}^T \begin{bmatrix} \overline{H}_1(\eta_1) & \cdots & \overline{H}_{n_\eta}(\eta_1) & \eta_1 & 1 \\ \overline{H}_1(\eta_2) & \cdots & \overline{H}_{n_\eta}(\eta_2) & \eta_2 & 1 \\ \vdots & \ddots & \vdots & \vdots & \vdots \\ \overline{H}_1(\eta_{n_\eta}) & \cdots & \overline{H}_{n_\eta}(\eta_{n_\eta}) & \eta_{n_\eta} & 1 \end{bmatrix}^{-1} \begin{pmatrix} u_1^n \\ u_2^n \\ \vdots \\ u_{n_\eta}^n \end{pmatrix}, \tag{40}$$

where $u_i = u(\eta_i)$ $(i \in \{1,2,\ldots,n_\eta\})$; and $\frac{d^2u_i}{d\eta^2} = \frac{d^2u}{d\eta^2}(\eta_i)$ $(i \in \{1,n_\eta\})$.
The IRBF system on a grid line for the second derivative of u is obtained by letting the interior node taking value from 2 to $(n_\eta - 1)$ in (39) and making use of (40)

$$\mathscr{L}_{\eta\eta}\widehat{u}_{\eta\eta}^n = \mathscr{B}_{\eta\eta}\widehat{u}^n, \tag{41}$$

where $\mathscr{L}_{\eta\eta}$, $\mathscr{B}_{\eta\eta}$ are $n_\eta \times n_\eta$ matrices.

3.1.2 CIRBF-2

First-order derivative compact approximations:

Unlike Scheme 1, nodal derivative values (*i.e.* extra information) used in the compact approximation of first derivatives are chosen here as $\frac{du_1}{d\eta}$ and $\frac{du_3}{d\eta}$. We construct the conversion system over a 3-point stencil associated with an interior node in the form of

$$\begin{pmatrix} u_1 \\ u_2 \\ u_3 \\ \frac{du_1}{d\eta} \\ \frac{du_3}{d\eta} \end{pmatrix} = \underbrace{\begin{pmatrix} \overline{\mathscr{H}} \\ \mathscr{H} \end{pmatrix}}_{\mathscr{C}_2} \begin{pmatrix} w_1 \\ w_2 \\ w_3 \\ c_1 \\ c_2 \end{pmatrix}, \tag{42}$$

where $\frac{du_i}{d\eta} = \frac{du}{d\eta}(\eta_i)$ $(i \in \{1,3\})$; $\mathscr{C}_2$ is the conversion matrix; $\overline{\mathscr{H}}$ is defined as before; and

$$\mathscr{H} = \begin{bmatrix} H_1(\eta_1) & H_2(\eta_1) & H_3(\eta_1) & 1 & 0 \\ H_1(\eta_3) & H_2(\eta_3) & H_3(\eta_3) & 1 & 0 \end{bmatrix}. \tag{43}$$

Solving (42) yields

$$\begin{pmatrix} w_1 \\ w_2 \\ w_3 \\ c_1 \\ c_2 \end{pmatrix} = \mathscr{C}_2^{-1} \begin{pmatrix} u_1 \\ u_2 \\ u_3 \\ \frac{du_1}{d\eta} \\ \frac{du_3}{d\eta} \end{pmatrix}, \tag{44}$$

which maps the vector of nodal values of the function and of its first-order derivative to the vector of RBF coefficients including the two integration constants. Approximate expressions for the first-order derivatives in the physical space are obtained by substituting (44) into (20)

$$\frac{du(\eta)}{d\eta} = \begin{bmatrix} H_1(\eta) & H_2(\eta) & H_3(\eta) & 1 & 0 \end{bmatrix} \mathscr{C}_2^{-1} \begin{pmatrix} \widehat{u} \\ \widehat{\frac{du}{d\eta}} \end{pmatrix}, \tag{45}$$

where $\eta_1 \leq \eta \leq \eta_3$; $\widehat{u} = (u_1, u_2, u_3)^T$ and $\widehat{\frac{du}{d\eta}} = (\frac{du_1}{d\eta}, \frac{du_3}{d\eta})^T$.
It can be rewritten as

$$\frac{du(\eta)}{d\eta} = \sum_{i=1}^{3} \frac{d\phi_i(\eta)}{d\eta} u_i + \frac{d\phi_4(\eta)}{d\eta} \frac{du_1}{d\eta} + \frac{d\phi_5(\eta)}{d\eta} \frac{du_3}{d\eta}, \tag{46}$$

where $\{\phi_i(\eta)\}_{i=1}^5$ is the set of IRBFs in the physical space.
At the current time level, equation (46) is taken as

$$\frac{du^n(\eta)}{d\eta} = \sum_{i=1}^{3} \frac{d\phi_i(\eta)}{d\eta} u_i^n + \frac{d\phi_4(\eta)}{d\eta} \frac{du_1^n}{d\eta} + \frac{d\phi_5(\eta)}{d\eta} \frac{du_3^n}{d\eta}, \tag{47}$$

where nodal values of the first-order derivatives on the right hand side are treated as unknowns.
Collocating (47) at $\eta = \eta_2$ results in

$$-\frac{d\phi_4(\eta_2)}{d\eta} \frac{du_1^n}{d\eta} + \frac{du_2^n}{d\eta} - \frac{d\phi_5(\eta_2)}{d\eta} \frac{du_3^n}{d\eta} = \frac{d\phi_1(\eta_2)}{d\eta} u_1^n + \frac{d\phi_2(\eta_2)}{d\eta} u_2^n + \frac{d\phi_3(\eta_2)}{d\eta} u_3^n, \tag{48}$$

or in matrix-vector form

$$\begin{bmatrix} -\frac{d\phi_4(\eta_2)}{d\eta} & 1 & -\frac{d\phi_5(\eta_2)}{d\eta} \end{bmatrix} \begin{bmatrix} \frac{du_1^n}{d\eta} \\ \frac{du_2^n}{d\eta} \\ \frac{du_3^n}{d\eta} \end{bmatrix} = \begin{bmatrix} \frac{d\phi_1(\eta_2)}{d\eta} & \frac{d\phi_2(\eta_2)}{d\eta} & \frac{d\phi_3(\eta_2)}{d\eta} \end{bmatrix} \begin{bmatrix} u_1^n \\ u_2^n \\ u_3^n \end{bmatrix}. \quad (49)$$

Figure 3: Special compact 4-point 1D-IRBF stencils for left and right boundary nodes

At the boundary nodes, instead of using the global 1D-IRBF approach as in Scheme 1, we compute the first derivative here using special compact local stencils (Figure 3). These proposed stencils are constructed as follows. Consider the boundary node η_1. Its associated stencil is $[\eta_1, \eta_2, \eta_3, \eta_4]$. The conversion system over this stencil is presented as the following matrix-vector multiplication

$$\begin{pmatrix} u_1 \\ u_2 \\ u_3 \\ u_4 \\ \frac{du_2}{d\eta} \end{pmatrix} = \underbrace{\begin{pmatrix} \overline{\mathscr{H}_{sp}} \\ \mathscr{H}_{sp} \end{pmatrix}}_{\mathscr{C}_{sp_1}} \begin{pmatrix} w_1 \\ w_2 \\ w_3 \\ w_4 \\ c_1 \\ c_2 \end{pmatrix}, \quad (50)$$

where $\mathscr{C}_{sp_1}$ is the conversion matrix and $\overline{\mathscr{H}_{sp}}$, $\mathscr{H}_{sp}$ are matrices defined as

$$\overline{\mathscr{H}_{sp}} = \begin{bmatrix} \overline{H}_1(\eta_1) & \overline{H}_2(\eta_1) & \overline{H}_3(\eta_1) & \overline{H}_4(\eta_1) & \eta_1 & 1 \\ \overline{H}_1(\eta_2) & \overline{H}_2(\eta_2) & \overline{H}_3(\eta_2) & \overline{H}_4(\eta_2) & \eta_2 & 1 \\ \overline{H}_1(\eta_3) & \overline{H}_2(\eta_3) & \overline{H}_3(\eta_3) & \overline{H}_4(\eta_3) & \eta_3 & 1 \\ \overline{H}_1(\eta_4) & \overline{H}_2(\eta_4) & \overline{H}_3(\eta_4) & \overline{H}_4(\eta_4) & \eta_4 & 1 \end{bmatrix}, \quad (51)$$

$$\mathscr{H}_{sp} = \begin{bmatrix} H_1(\eta_2) & H_2(\eta_2) & H_3(\eta_2) & H_4(\eta_2) & 1 & 0 \end{bmatrix}. \quad (52)$$

Solving (50) yields

$$\begin{pmatrix} w_1 \\ w_2 \\ w_3 \\ w_4 \\ c_1 \\ c_2 \end{pmatrix} = \mathscr{C}_{sp_1}^{-1} \begin{pmatrix} u_1 \\ u_2 \\ u_3 \\ u_4 \\ \frac{du_2}{d\eta} \end{pmatrix}. \tag{53}$$

The boundary value of the first-order derivative of u is thus obtained by substituting (53) into (20) and taking $\eta = \eta_1$

$$\frac{du(\eta_1)}{d\eta} = \begin{bmatrix} H_1(\eta_1) & H_2(\eta_1) & H_3(\eta_1) & H_4(\eta_1) & 1 & 0 \end{bmatrix} \mathscr{C}_{sp_1}^{-1} \begin{pmatrix} u_1 & u_2 & u_3 & u_4 & \frac{du_2}{d\eta} \end{pmatrix}^T, \tag{54}$$

or

$$\frac{du_1^n}{d\eta} - \frac{d\phi_{sp_5}(\eta_1)}{d\eta}\frac{du_2^n}{d\eta} = \frac{d\phi_{sp_1}(\eta_1)}{d\eta}u_1^n + \frac{d\phi_{sp_2}(\eta_1)}{d\eta}u_2^n + \frac{d\phi_{sp_3}(\eta_1)}{d\eta}u_3^n + \frac{d\phi_{sp_4}(\eta_1)}{d\eta}u_4^n, \tag{55}$$

where $\{\phi_{sp_i}(\eta)\}_{i=1}^5$ is the set of IRBFs in the physical space. We rewrite equation (55) in matrix-vector form

$$\begin{bmatrix} 1 & -\frac{d\phi_{sp_5}(\eta_1)}{d\eta} & 0 & 0 \end{bmatrix} \begin{bmatrix} \frac{du_1^n}{d\eta} \\ \frac{du_2^n}{d\eta} \\ \frac{du_3^n}{d\eta} \\ \frac{du_4^n}{d\eta} \end{bmatrix} = \begin{bmatrix} \frac{d\phi_{sp_1}(\eta_1)}{d\eta} & \frac{d\phi_{sp_2}(\eta_1)}{d\eta} & \frac{d\phi_{sp_3}(\eta_1)}{d\eta} & \frac{d\phi_{sp_4}(\eta_1)}{d\eta} \end{bmatrix} \begin{bmatrix} u_1^n \\ u_2^n \\ u_3^n \\ u_4^n \end{bmatrix}. \tag{56}$$

In a similar manner, one is able to calculate the first derivative of u at the boundary node η_{n_η}.

The IRBF system on a grid line for the first derivative of u is obtained by letting the interior node taking value from 2 to $(n_\eta - 1)$ in (49) and making use of (56),

$$\mathscr{L}_\eta \widehat{u}_\eta^n = \mathscr{A}_\eta \widehat{u}^n. \tag{57}$$

Second-order derivative compact approximations:

Nodal derivative values (*i.e.* extra information) used in the compact approximation of second-order derivatives are chosen here as $\frac{d^2u_1}{d\eta^2}$ and $\frac{d^2u_3}{d\eta^2}$. The corresponding formulation is thus exactly the same as described in Scheme 1 (*i.e.* (39)). However, at the boundary nodes, instead of using the global 1D-IRBF approach as in Scheme 1, we compute the second-order derivative here using special compact local stencils (Figure 3). Consider the boundary node, *e.g.*, η_1. The conversion system over the associated stencil is presented as the following matrix-vector multiplication

$$\begin{pmatrix} u_1 \\ u_2 \\ u_3 \\ u_4 \\ \frac{d^2u_2}{d\eta^2} \end{pmatrix} = \underbrace{\begin{pmatrix} \overline{\mathscr{H}_{sp}} \\ \mathscr{G}_{sp} \end{pmatrix}}_{\mathscr{C}_{sp_2}} \begin{pmatrix} w_1 \\ w_2 \\ w_3 \\ w_4 \\ c_1 \\ c_2 \end{pmatrix}, \tag{58}$$

where $\mathscr{C}_{sp_2}$ is the conversion matrix; $\overline{\mathscr{H}_{sp}}$ is defined as before; and

$$\mathscr{G}_{sp} = \begin{bmatrix} G_1(\eta_2) & G_2(\eta_2) & G_3(\eta_2) & G_4(\eta_2) & 0 & 0 \end{bmatrix}. \tag{59}$$

Solving (58) yields

$$\begin{pmatrix} w_1 \\ w_2 \\ w_3 \\ w_4 \\ c_1 \\ c_2 \end{pmatrix} = \mathscr{C}_{sp_2}^{-1} \begin{pmatrix} u_1 \\ u_2 \\ u_3 \\ u_4 \\ \frac{d^2u_2}{d\eta^2} \end{pmatrix}. \tag{60}$$

The boundary value of the second-order derivative of u is thus obtained by substituting (60) into (19) and taking $\eta = \eta_1$

$$\frac{d^2u(\eta_1)}{d\eta^2} = \begin{bmatrix} G_1(\eta_1) & G_2(\eta_1) & G_3(\eta_1) & G_4(\eta_1) & 0 & 0 \end{bmatrix} \mathscr{C}_{sp_2}^{-1} \begin{pmatrix} u_1 & u_2 & u_3 & u_4 & \frac{d^2u_2}{d\eta^2} \end{pmatrix}^T, \tag{61}$$

or

$$\frac{d^2u_1^n}{d\eta^2} - \frac{d^2\varphi_{sp_5}(\eta_1)}{d\eta^2}\frac{d^2u_2^n}{d\eta^2} = \frac{d^2\varphi_{sp_1}(\eta_1)}{d\eta^2}u_1^n + \frac{d^2\varphi_{sp_2}(\eta_1)}{d\eta^2}u_2^n + \frac{d^2\varphi_{sp_3}(\eta_1)}{d\eta^2}u_3^n + \frac{d^2\varphi_{sp_4}(\eta_1)}{d\eta^2}u_4^n, \tag{62}$$

where $\{\varphi_{sp_i}(\eta)\}_{i=1}^{5}$ is the set of IRBFs in the physical space. We rewrite equation (62) in matrix-vector form

$$\begin{bmatrix} 1 & -\frac{d^2\varphi_{sp_5}(\eta_1)}{d\eta^2} & 0 & 0 \end{bmatrix} \begin{bmatrix} \frac{d^2u_1^n}{d\eta^2} \\ \frac{d^2u_2^n}{d\eta^2} \\ \frac{d^2u_3^n}{d\eta^2} \\ \frac{d^2u_4^n}{d\eta^2} \end{bmatrix} = \begin{bmatrix} \frac{d^2\varphi_{sp_1}(\eta_1)}{d\eta^2} & \frac{d^2\varphi_{sp_2}(\eta_1)}{d\eta^2} & \frac{d^2\varphi_{sp_3}(\eta_1)}{d\eta^2} & \frac{d^2\varphi_{sp_4}(\eta_1)}{d\eta^2} \end{bmatrix} \begin{bmatrix} u_1^n \\ u_2^n \\ u_3^n \\ u_4^n \end{bmatrix}. \quad (63)$$

The IRBF system on a grid line for the second derivative of u is obtained by letting the interior node taking value from 2 to $(n_\eta - 1)$ in (39) and making use of (63),

$$\mathscr{L}_{\eta\eta}\widehat{u}_{\eta\eta}^n = \mathscr{B}_{\eta\eta}\widehat{u}^n, \quad (64)$$

where $\mathscr{L}_{\eta\eta}$, $\mathscr{B}_{\eta\eta}$ are $n_\eta \times n_\eta$ matrices.

It is noted that, for brevity, we use the same notations to represent the RBF coefficients and the coefficient matrices for the two schemes and also for the approximation of first and second derivatives in Scheme 2. In fact, for example, the entries of $\mathscr{L}_\eta$, $\mathscr{L}_{\eta\eta}$, $\mathscr{A}_\eta$ and $\mathscr{B}_{\eta\eta}$ in (57) and (64) are different from those of $\mathscr{L}_\eta$, $\mathscr{L}_{\eta\eta}$, $\mathscr{A}_\eta$ and $\mathscr{B}_{\eta\eta}$ in (32) and (41); and the coefficient set (w_1, w_2, w_3, w_4, c_1, c_2) in (50) is not the same as that in (58).

3.2 Temporal discretisation

The temporal discretisation of (1) with a Crank-Nicolson scheme [Crank and Nicolson (1996)] gives

$$\begin{aligned} u^n + \frac{\Delta t}{2}c_x\frac{\partial u^n}{\partial x} - \frac{\Delta t}{2}d_x\frac{\partial^2 u^n}{\partial x^2} + \frac{\Delta t}{2}c_y\frac{\partial u^n}{\partial y} - \frac{\Delta t}{2}d_y\frac{\partial^2 u^n}{\partial y^2} \\ = u^{n-1} - \frac{\Delta t}{2}c_x\frac{\partial u^{n-1}}{\partial x} + \frac{\Delta t}{2}d_x\frac{\partial^2 u^{n-1}}{\partial x^2} - \frac{\Delta t}{2}c_y\frac{\partial u^{n-1}}{\partial y} + \frac{\Delta t}{2}d_y\frac{\partial^2 u^{n-1}}{\partial y^2} \\ + \Delta t f_b^{n-1/2} + \mathscr{O}(\Delta t^2). \end{aligned} \quad (65)$$

We apply the ADI factorisation to (65), resulting in

$$\left\{1+\frac{\Delta t}{2}c_x\frac{\partial}{\partial x}-\frac{\Delta t}{2}d_x\frac{\partial^2}{\partial x^2}\right\}\left\{1+\frac{\Delta t}{2}c_y\frac{\partial}{\partial y}-\frac{\Delta t}{2}d_y\frac{\partial^2}{\partial y^2}\right\}u^n$$
$$=\left\{1-\frac{\Delta t}{2}c_x\frac{\partial}{\partial x}+\frac{\Delta t}{2}d_x\frac{\partial^2}{\partial x^2}\right\}\left\{1-\frac{\Delta t}{2}c_y\frac{\partial}{\partial y}+\frac{\Delta t}{2}d_y\frac{\partial^2}{\partial y^2}\right\}u^{n-1}$$
$$+\Delta t f_b^{n-1/2}+\mathscr{O}(\Delta t^2). \quad (66)$$

Equation (66) can be further factorised as

$$\left(1+\frac{\Delta t}{2}c_x\frac{\partial}{\partial x}\right)\left(1-\frac{\Delta t}{2}d_x\frac{\partial^2}{\partial x^2}\right)\left(1+\frac{\Delta t}{2}c_y\frac{\partial}{\partial y}\right)\left(1-\frac{\Delta t}{2}d_y\frac{\partial^2}{\partial y^2}\right)u^n$$
$$=\left(1-\frac{\Delta t}{2}c_x\frac{\partial}{\partial x}\right)\left(1+\frac{\Delta t}{2}d_x\frac{\partial^2}{\partial x^2}\right)\left(1-\frac{\Delta t}{2}c_y\frac{\partial}{\partial y}\right)\left(1+\frac{\Delta t}{2}d_y\frac{\partial^2}{\partial y^2}\right)u^{n-1}$$
$$+\Delta t f_b^{n-1/2}+\mathscr{O}(\Delta t^2). \quad (67)$$

It is noted that Equations (66) and (67) have the same order accuracy in time (*i.e.* second order) as Equation (65).

3.3 Spatial - temporal discretisation

Incorporation of the CIRBF approximations derived in Section 3.3.1 (*i.e.* CIRBF-1) and 3.3.2 (*i.e.* CIRBF-2) into the ADI equation (67) leads to, respectively, the following two schemes

3.3.1 ADI-CIRBF-1

From (32) and (41), nodal values of the first- and second-order derivatives of u can be derived in terms of nodal variable values

$$\widehat{u}_\eta=\mathscr{L}_\eta^{-1}\left(\mathscr{A}_\eta+\mathscr{A}_{\eta\eta}\mathscr{L}_{\eta\eta}^{-1}\mathscr{B}_{\eta\eta}\right)\widehat{u}, \quad (68)$$

$$\widehat{u}_{\eta\eta}=\mathscr{L}_{\eta\eta}^{-1}\mathscr{B}_{\eta\eta}\widehat{u}. \quad (69)$$

Substituting (68) and (69) into (67) results in

$$\mathscr{L}_x^{-1}\mathscr{T}_x^+\mathscr{L}_{xx}^{-1}\mathscr{T}_{xx}^-\mathscr{L}_y^{-1}\mathscr{T}_y^+\mathscr{L}_{yy}^{-1}\mathscr{T}_{yy}^-\widehat{u}^n=$$
$$\mathscr{L}_x^{-1}\mathscr{T}_x^-\mathscr{L}_{xx}^{-1}\mathscr{T}_{xx}^+\mathscr{L}_y^{-1}\mathscr{T}_y^-\mathscr{L}_{yy}^{-1}\mathscr{T}_{yy}^+\widehat{u}^{n-1}+\Delta t\widehat{f}_b^{n-1/2}, \quad (70)$$

where

$$\mathscr{T}_x^{\pm} = \left(\mathscr{L}_x \pm \frac{\Delta t}{2} c_x \left\{ \mathscr{A}_x + \mathscr{A}_{xx} \mathscr{L}_{xx}^{-1} \mathscr{B}_{xx} \right\} \right), \qquad \mathscr{T}_{xx}^{\pm} = \left(\mathscr{L}_{xx} \pm \frac{\Delta t}{2} d_x \mathscr{B}_{xx} \right), \quad (71)$$

$$\mathscr{T}_y^{\pm} = \left(\mathscr{L}_y \pm \frac{\Delta t}{2} c_y \left\{ \mathscr{A}_y + \mathscr{A}_{yy} \mathscr{L}_{yy}^{-1} \mathscr{B}_{yy} \right\} \right), \qquad \mathscr{T}_{yy}^{\pm} = \left(\mathscr{L}_{yy} \pm \frac{\Delta t}{2} d_y \mathscr{B}_{yy} \right).$$

3.3.2 ADI-CIRBF-2

From (57) and (64), nodal values of the first- and second-order derivatives of u can be derived in terms of nodal variable values

$$\widehat{u}_\eta = \mathscr{L}_\eta^{-1} \mathscr{A}_\eta \widehat{u}, \quad (72)$$

$$\widehat{u}_{\eta\eta} = \mathscr{L}_{\eta\eta}^{-1} \mathscr{B}_{\eta\eta} \widehat{u}. \quad (73)$$

Substituting (72) and (73) into (67) results in

$$\mathscr{L}_x^{-1} \mathscr{T}_x^{+} \mathscr{L}_{xx}^{-1} \mathscr{T}_{xx}^{-} \mathscr{L}_y^{-1} \mathscr{T}_y^{+} \mathscr{L}_{yy}^{-1} \mathscr{T}_{yy}^{-} \widehat{u}^n = \mathscr{L}_x^{-1} \mathscr{T}_x^{-} \mathscr{L}_{xx}^{-1} \mathscr{T}_{xx}^{+} \mathscr{L}_y^{-1} \mathscr{T}_y^{-} \mathscr{L}_{yy}^{-1} \mathscr{T}_{yy}^{+} \widehat{u}^{n-1} + \Delta t \widehat{f}_b^{n-1/2}, \quad (74)$$

where

$$\mathscr{T}_x^{\pm} = \left(\mathscr{L}_x \pm \frac{\Delta t}{2} c_x \mathscr{A}_x \right), \qquad \mathscr{T}_{xx}^{\pm} = \left(\mathscr{L}_{xx} \pm \frac{\Delta t}{2} d_x \mathscr{B}_{xx} \right), \quad (75)$$

$$\mathscr{T}_y^{\pm} = \left(\mathscr{L}_y \pm \frac{\Delta t}{2} c_y \mathscr{A}_y \right), \qquad \mathscr{T}_{yy}^{\pm} = \left(\mathscr{L}_{yy} \pm \frac{\Delta t}{2} d_y \mathscr{B}_{yy} \right).$$

3.3.3 Calculation procedure

Equation (70)/(74) is equivalent to

$$\mathscr{L}_x^{-1} \mathscr{T}_x^{+} \mathscr{L}_{xx}^{-1} \mathscr{T}_{xx}^{-} \widehat{u}^* = \mathscr{L}_x^{-1} \mathscr{T}_x^{-} \mathscr{L}_{xx}^{-1} \mathscr{T}_{xx}^{+} \mathscr{L}_y^{-1} \mathscr{T}_y^{-} \mathscr{L}_{yy}^{-1} \mathscr{T}_{yy}^{+} \widehat{u}^{n-1} + \Delta t \widehat{f}_b^{n-1/2}, \quad (76)$$

$$\mathscr{L}_y^{-1} \mathscr{T}_y^{+} \mathscr{L}_{yy}^{-1} \mathscr{T}_{yy}^{-} \widehat{u}^n = \widehat{u}^*, \quad (77)$$

which can be solved by the following two steps.

Step 1: This step involves two substeps

- Substep 1: Compute the nodal values of u^* at the left and right boundaries of the computational domain via equation (77) for $x = x_1$ and $x = x_{n_x}$ with the given boundary condition (3).

- Substep 2: Solve equation (76) on the x-grid lines ($y = y_j,\ j \in \{2,3,\cdots,n_y-1\}$) for the values of u^* at the interior nodes.

Step 2: Solve (77) on the y-grid lines ($x = x_i,\ i \in \{2,3,\cdots,n_x-1\}$) for the values of u^n at the interior nodes.

Owing to the ADI technique, the computational costs for the two present solution procedures are low. Scheme 2 (*i.e.* ADI-CIRBF-2) is more efficient as only local stencils are involved.

4 Numerical examples

It has generally been accepted that, among RBFs, the multiquadric (MQ) function tends to result in the most accurate approximation [Franke (1982)]. We choose MQ as the basis function in the present calculations

$$G_i(\widehat{x}) = \sqrt{(\widehat{x}-\widehat{c}_i)^T(\widehat{x}-\widehat{c}_i)+a_i^2}, \tag{78}$$

where $\widehat{x} = (x,y)^T$ is the position vector of the point of interest; and $\widehat{c}_i = (x_{c_i}, y_{c_i})^T$ and a_i the position vector of the centre and the width of the ith MQ, respectively. For each stencil, the set of nodal points is taken to be the set of MQ centres. We simply choose the MQ width as $a_i = \beta h_i$ in which h_i the distance between the ith node and its nearest neighbouring node and β is a given positive number: $\beta = 1$ for global stencils and $\beta = 50$ for local stencils in Scheme 1 and Scheme 2. We assess the performance of the proposed scheme through the following measures:

(i) the average absolute error (L_1) defined as

$$L_1 = \frac{1}{N}\sum_{i=1}^{N}|u_i - \overline{u}_i|, \tag{79}$$

where N is the number of nodes over the whole domain and $\overline{u}$ is the analytic solution,

(ii) the root mean square error (RMS) defined as

$$RMS = \sqrt{\frac{\sum_{i=1}^{N}(u_i-\overline{u}_i)^2}{N}}, \tag{80}$$

(iii) the maximum absolute error (L_∞) defined as

$$L_\infty = \max_i |u_i - \overline{u}_i|, \tag{81}$$

(iv) the grid convergence behaviour $O(h^{\alpha})$, where α is the average convergence rate, determined in the least square sense. Local convergence rates are given by

$$\alpha = \frac{\log(RMS^{(r)}/RMS^{(s)})}{\log(h^{(r)}/h^{(s)})}, \tag{82}$$

in which h is the grid size; and the superscripts (r) and (s) indicate the data obtained from computations with the rth and sth grid, respectively.

A flow is considered to reach its steady state when

$$\sqrt{\frac{\sum_{i=1}^{N}(u_i^{n+1}-u_i^n)^2}{N}} < 10^{-9}. \tag{83}$$

4.1 Unsteady diffusion equation

Consider a diffusion equation by setting the parameters in Equation (1) as $c_x = c_y = 0$, $d_x = d_y = 1$ and $f_b = 0$. The analytic solution is taken here as [Tian and Ge (2007)]

$$\overline{u}(x,y,t) = e^{-2\pi^2 t}\sin(\pi x)\sin(\pi y). \tag{84}$$

The problem domain is chosen to be a unit square $\Omega = [0,1]\times[0,1]$ and the initial and Dirichlet boundary conditions are derived from (84).

We employ a set of uniform grids to study the convergence of the solution with grid refinement. Results obtained at $t = 0.0125$ using $\Delta t = 10^{-5}$ and $\{11\times 11, 16\times 16, \ldots, 41\times 41\}$ are displayed in Figure 4, showing that the approximate solution converges apparently as $O(h^{2.74})$ for ADI-CIRBF-1, and $O(h^{4.76})$ for ADI-CIRBF-2.

We employ a set of time steps $\Delta t = \{0.05, 0.025, 0.0125, 0.00625\}$ to test the temporal accuracy. Results obtained at $t = 1.25$ using an uniform grid of 81×81 are shown in in Table 1. The two present schemes are about second-order accurate in time as expected (temporal derivative terms are presently discretised with a second-order Crank-Nicolson scheme). It is noted that we employ a fine grid of 81×81 to ensure that the approximate error in space is small enough so that its effects can be neglected.

To facilitate a comparison with the exponential high-order compact ADI scheme (EHOC-ADI) [Tian and Ge (2007)], we now choose $\Delta t = h^2$ and $t = 0.125$. Table 2 indicates that the present ADI-CIRBF-2 scheme and the EHOC-ADI scheme yield similar local rates of convergence of about 4.

Figure 5 plots the *RMS* error against time with $\Delta t = 10^{-4}$. It can be seen that ADI-CIRBF-2 is the most accurate scheme, followed by ADI-CIRBF-1 and then

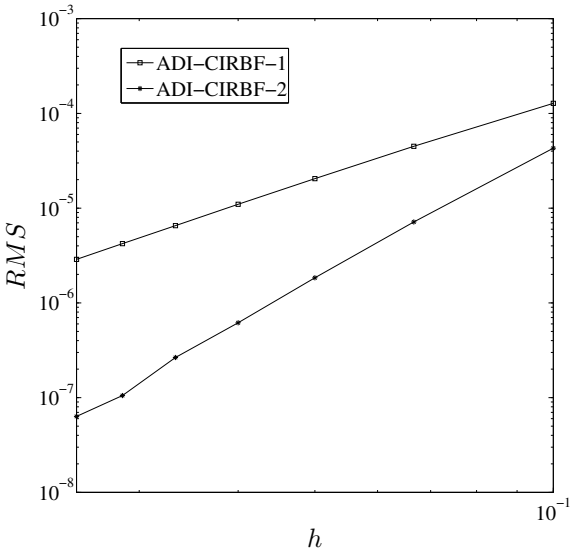

Figure 4: Unsteady diffusion equation, $\{11\times 11, 16\times 16, \ldots, 41\times 41\}$, $\Delta t = 10^{-5}$, $t = 0.0125$: The effect of grid size h on the solution accuracy for the two present schemes. The solution converges as $O(h^{2.74})$ for ADI-CIRBF-1 and $O(h^{4.76})$ for ADI-CIRBF-2.

PR-ADI. It also shows that the present results using a grid of 21×21 are already more accurate than the standard ADI results using a grid of 41×41.

4.2 Unsteady convection-diffusion equation

Consider the unsteady convection-diffusion equation (1), where $f_b = 0$, in a square $\Omega = [0,2]\times[0,2]$ with the following analytic solution [Noye and Tan (1989)]

$$\overline{u}(x,y,t) = \frac{1}{4t+1} exp\left[-\frac{(x-c_x t-0.5)^2}{d_x(4t+1)} - \frac{(y-c_y t-0.5)^2}{d_y(4t+1)}\right], \tag{85}$$

and subject to Dirichlet boundary conditions. From (85), one can derive the initial and boundary conditions.

Figure 6 shows the accuracy of the spatial discretisation of the two present schemes. The calculations are carried out on a set of uniform grids $\{31\times 31, 41\times 41, \ldots, 81\times 81\}$ and a time step of 10^{-4} with the following parameters: $c_x = c_y = 0.8$, $d_x = d_y = 0.01$. The accuracy of the solution is measured at $t = 1.25$. It is noted that the time step is chosen small enough to minimise the effect of the approximate error in time.

Table 1: Unsteady diffusion equation, $t = 1.25$, grid 81×81: Solution accuracy of the two present schemes against time step.

	ADI-CIRBF-1		ADI-CIRBF-2	
Δt	*RMS*	Local Rate	*RMS*	Local Rate
0.05	3.8700E-12	—-	3.8518E-12	—-
0.025	1.1432E-12	1.76	1.1276E-12	1.77
0.0125	2.9542E-13	1.95	2.9337E-13	1.94
0.00625	7.3686E-14	2.00	7.4054E-14	1.99

Table 2: Unsteady diffusion equation, $t = 0.125$, $\Delta t = h^2$: Effect of grid size on the solution accuracy.

	EHOC-ADI		ADI-CIRBF-2	
Grid ($n_x \times n_y$)	*RMS*	Local Rate	*RMS*	Local Rate
11×11	8.55134E-05	—-	9.39417E-05	—-
21×21	5.19160E-06	4.041	5.81951E-06	4.013
41×41	3.17475E-07	4.031	4.02907E-07	3.852

Table 3: Unsteady convection-diffusion equation, grid 81×81, $t = 1.25$, $\Delta t = 0.00625$: Comparison of the solution accuracy between the present schemes and some other techniques.

Method	$L_1(u)$	$RMS(u)$	$L_\infty(u)$
PR-ADI [Peaceman and H. H. Rachford (1955)]	3.109E-04	2.025E-03	7.778E-03
3^{rd}-order 9-point compact [Noye and Tan (1989)]	1.971E-05	1.280E-04	6.509E-04
4^{th}-order 9-point compact [Kalita, Dalal, and Dass (2002)]	1.597E-05	1.024E-04	4.477E-04
HOC-ADI [Karaa and Zhang (2004)]	9.218E-06	5.931E-05	2.500E-04
EHOC-ADI [Tian and Ge (2007)]	9.663E-06	6.194E-05	2.664E-04
ADI-CIRBF-1	8.457E-06	2.808E-05	2.250E-04
ADI-CIRBF-2	6.742E-06	2.197E-05	1.703E-04

It can be seen that the solution converges very fast with grid refinement: $O(h^{4.07})$ for ADI-CIRBF-1 and $O(h^{4.32})$ for ADI-CIRBF-2. Figure 7 shows the initial pulse and the pulse at $t = 1.25$ using a grid of 81×81 and $\Delta t = 0.00625$ by the two present schemes. The initial pulse is a Gaussian pulse centred at $(0.5, 0.5)$ with the pulse height 1. At $t = 1.25$, the pulse moves to a position centred at $(1.5, 1.5)$ with the pulse height of $1/6$. Figure 8 displays the surface plots of the solution obtained by the analytic solution and the two present schemes in a sub-region $1 \leq x, y \leq 2$ - these plots are almost identical.

Table 3 shows a comparison of L_1, *RMS* and L_∞ errors between the two present schemes and the standard PR-ADI scheme, third-order nine-point compact scheme [Noye and Tan (1989)], fourth-order nine-point compact scheme [Kalita, Dalal,

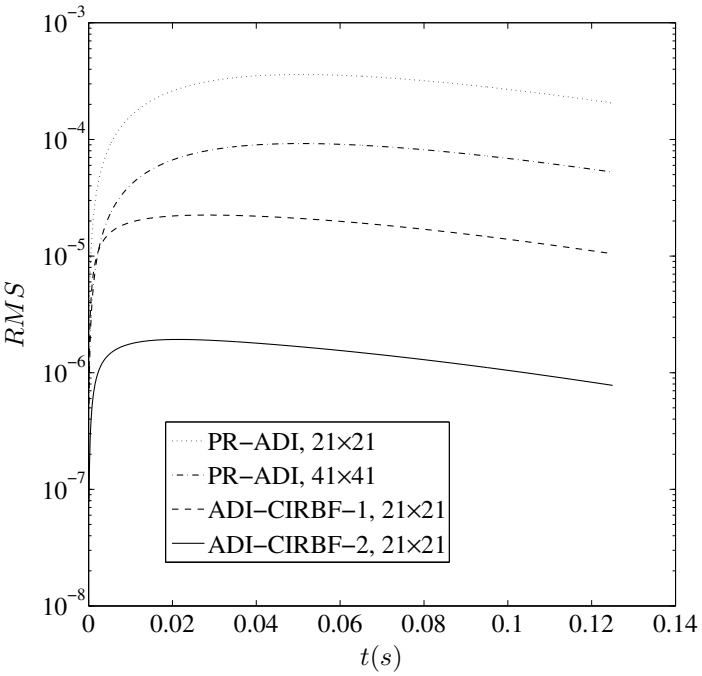

Figure 5: Unsteady diffusion equation, $\Delta t = 10^{-4}$: The solution accuracy of the standard PR-ADI and the two present schemes against time.

and Dass (2002)], HOC-ADI scheme [Karaa and Zhang (2004)] and exponential high-order compact ADI (EHOC-ADI) [Tian and Ge (2007)]. It can be seen that the present schemes yield solutions with higher accuracy. In addition, in Figure 9, we plot *RMS* against time for these schemes, except for EHOC-ADI (the data for this scheme is not available). It shows that all of these curves have similar shapes and the present schemes have smaller error for every time step. Figure 10 displays contour plots of the pulse in the region $1 \leq x, y \leq 2$ by the analytic solution, PR-ADI, ADI-CIRBF-1 and ADI-CIRBF-2. Contour plots of other mentioned schemes can be found in [Tian and Ge (2007)]. It can be seen that the computed pulses by the two present schemes are visually indistinguishable from the analytic one, while PR-ADI produces a pulse that is distorted in both x- and y-directions. For the latter, the reason was explained in [Noye and Tan (1989)] (the second-order error terms of the standard PR-ADI scheme are related to the wave numbers in both directions).

Recently, Ma, Sun, Haake, Churchill, and Ho (2012) proposed a high-order hybrid Pad' ADI (HPD-ADI) method for convection-dominated diffusion problems and

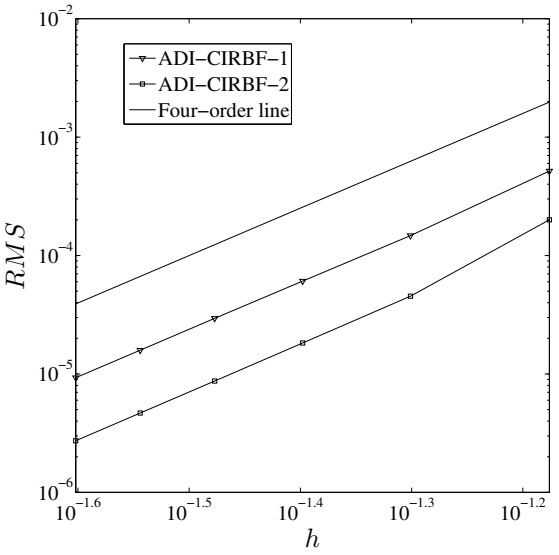

Figure 6: Unsteady convection-diffusion equation, $\{31\times 31, 41\times 41, \ldots, 81\times 81\}$, $\Delta t = 10^{-4}$, $t = 1.25$: The effect of grid size h on the solution accuracy for the two present schemes. The solution converges as $O(h^{4.07})$ for ADI-CIRBF-1 and $O(h^{4.32})$ for ADI-CIRBF-2.

also examined the performance of their method via this example. We consider two sets of parameters used in their article

Case I: $c_x = c_y = 0.8$, $d_x = d_y = 0.01$, $h = 0.025$, $t = 1.25$, $\Delta t = 2.5E-4$.

Case II: $c_x = c_y = 80$, $d_x = d_y = 0.01$, $h = 0.025$, $t = 0.0125$, $\Delta t = 2.5E-6$.

The corresponding Peclet number is thus $Pe = 2$ for Case I and $Pe = 200$ for Case II. Results concerning *RMS* and L_∞ errors are presented in Tables 4-6. In the case of low P_e, the two present schemes are superior to HPD-ADI and also other schemes (Table 4). In the case of high P_e (*i.e.* convection dominated), ADI-CIRBF-2 yields the best performance: higher degrees of accuracy (Table 5) and higher rates of convergence (Table 6).

4.3 Steady convection-diffusion equation

Consider Equation (4) with $c_x = c_y = 0.1$, $d_x = d_y = 1$ in a square $\Omega = [0, L]\times[0, L]$ and subject to Dirichlet boundary condition. The analytic solution takes the form

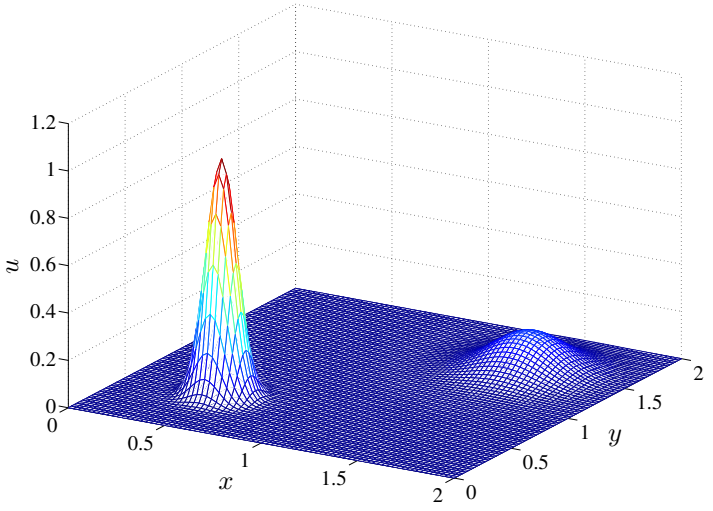

(a)

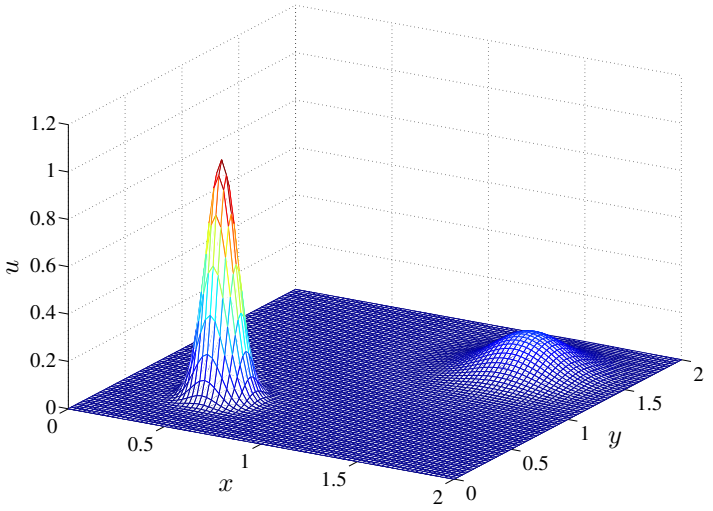

(b)

Figure 7: Unsteady convection-diffusion equation, 81×81, $\Delta t = 0.00625$: The initial and the computed pulses at $t = 1.25$ by ADI-CIRBF-1 (a) and ADI-CIRBF-2 (b).

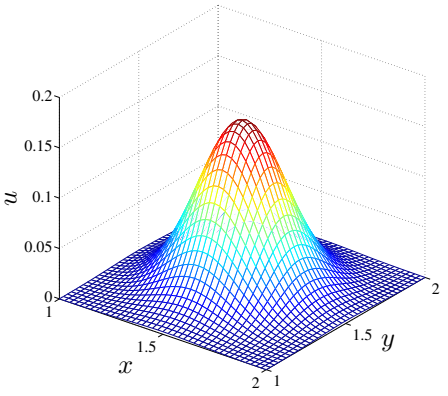

(a)

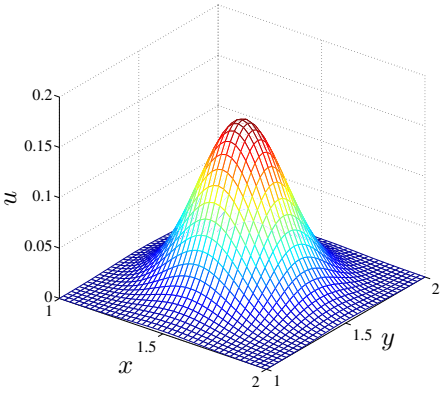

(b)

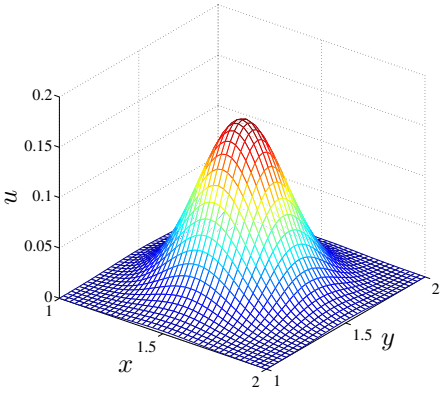

(c)

Figure 8: Unsteady convection-diffusion equation, 81×81, $\Delta t = 0.00625$: Surface plots of the pulse in the sub-region $1 \leq x, y \leq 2$ at $t = 1.25$ by the analytic solution (a), ADI-CIRBF-1 (b) and ADI-CIRBF-2 (c).

Table 4: Unsteady convection-diffusion equation, grid 81×81, $t = 1.25$, $\Delta t = 2.5E-4$: Comparison of the solution accuracy between the present schemes and some other techniques for case I.

Method	$RMS(u)$	$L_\infty(u)$
PR-ADI [Peaceman and H. H. Rachford (1955)]	1.11E-03	8.92E-03
HOC-ADI [Karaa and Zhang (2004)]	2.73E-05	2.46E-04
PDE-ADI [You (2006)]	2.20E-05	1.71E-04
HPD-ADI [Ma, Sun, Haake, Churchill, and Ho (2012)]	6.38E-05	6.54E-04
ADI-CIRBF-1	9.32E-06	7.80E-05
ADI-CIRBF-2	2.75E-06	2.37E-05

Table 5: Unsteady convection-diffusion equation, grid 81×81, $t = 0.0125$, $\Delta t = 2.5E-6$: Comparison of the solution accuracy between the present schemes and some other techniques for case II.

Method	$RMS(u)$	$L_\infty(u)$
PR-ADI [Peaceman and H. H. Rachford (1955)]	2.69E-02	3.74E-01
HOC-ADI [Karaa and Zhang (2004)]	1.47E-02	2.42E-01
PDE-ADI [You (2006)]	5.49E-04	1.22E-02
HPD-ADI [Ma, Sun, Haake, Churchill, and Ho (2012)]	5.49E-04	1.24E-02
ADI-CIRBF-1	1.71E-03	3.32E-02
ADI-CIRBF-2	5.45E-04	1.06E-02

Table 6: Unsteady convection-diffusion equation, $t = 0.0125$, $\Delta t = 2.5E-6$: The solution accuracy of the present schemes and some other techniques against grid size for case II. LCR stands for “local convergence rate".

	PDE-ADI		HPD-ADI		ADI-CIRBF-1		ADI-CIRBF-2	
Grid ($n_x \times n_y$)	$RMS(n_x)$	LCR	$RMS(n_x)$	LCR	$RMS(n_x)$	LCR	$RMS(n_x)$	LCR
31×31	1.93E-02	—-	1.91E-02	—-	3.22E-02	—-	2.42E-02	—-
41×41	8.41E-03	2.98	8.30E-03	2.97	1.69E-02	2.29	8.45E-03	3.45
51×51	3.74E-03	3.30	3.70E-03	3.29	9.14E-03	2.52	3.74E-03	3.58
61×61	1.80E-03	3.51	1.78E-03	3.50	5.00E-03	2.75	1.79E-03	3.71
71×71	9.51E-04	3.63	9.48E-04	3.62	2.85E-03	2.92	9.47E-04	3.80
81×81	5.49E-04	3.69	5.49E-04	3.69	1.71E-03	3.05	5.45E-04	3.86
101×101	2.21E-04	3.78	2.23E-04	3.76	7.14E-04	3.22	2.18E-04	3.91
121×121	1.07E-04	3.81	1.10E-04	3.79	3.46E-04	3.33	1.04E-04	3.94

LCR=-log[RMS(n_x)/RMS(31)]/log[n_x/31].

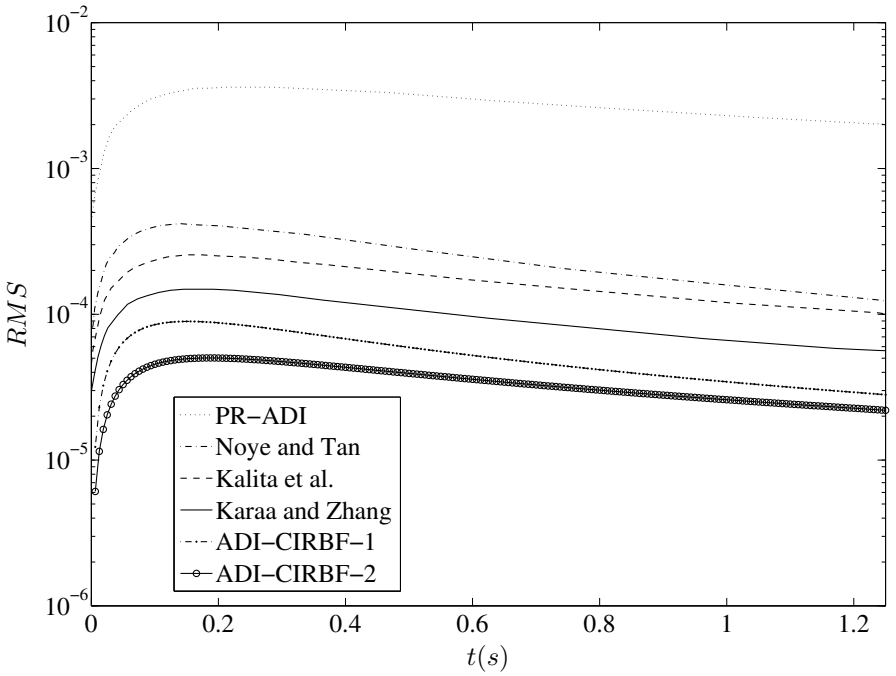

Figure 9: Unsteady convection-diffusion equation, 81×81, $\Delta t = 0.00625$: The solution accuracy of the present schemes and some other techniques against time.

[Sheu, Kao, Chiu, and Lin (2011)]

$$\overline{u} = \frac{u_0}{e^{r_+} - e^{r_-}} e^{\delta_x/2} \sin(\pi x) \left(e^{r_+ y} - e^{r_- y}\right), \tag{86}$$

where $u_0 = 1$, $\delta_x = c_x L/d_x$, $\delta_y = c_y L/d_y$, $L = 1$, and

$$r_\pm = \frac{1}{2}\delta_y \pm \frac{1}{2}\sqrt{\left(\delta_y^2 + 4W\right)}, \quad W = 4\pi^2 + \delta_x^2/4. \tag{87}$$

The driving function f_b is given by

$$f_b = c_x \frac{\partial \overline{u}}{\partial x} + c_y \frac{\partial \overline{u}}{\partial y} - d_x \frac{\partial^2 \overline{u}}{\partial x^2} - d_y \frac{\partial^2 \overline{u}}{\partial y^2}. \tag{88}$$

To solve the steady equation (4), a pseudo time-derivative term $\frac{\partial u}{\partial t}$ is added to its left side to facilitate an iterative calculation. The steady equation (4) thus has the same form as the unsteady equation (1). When the difference of u between two

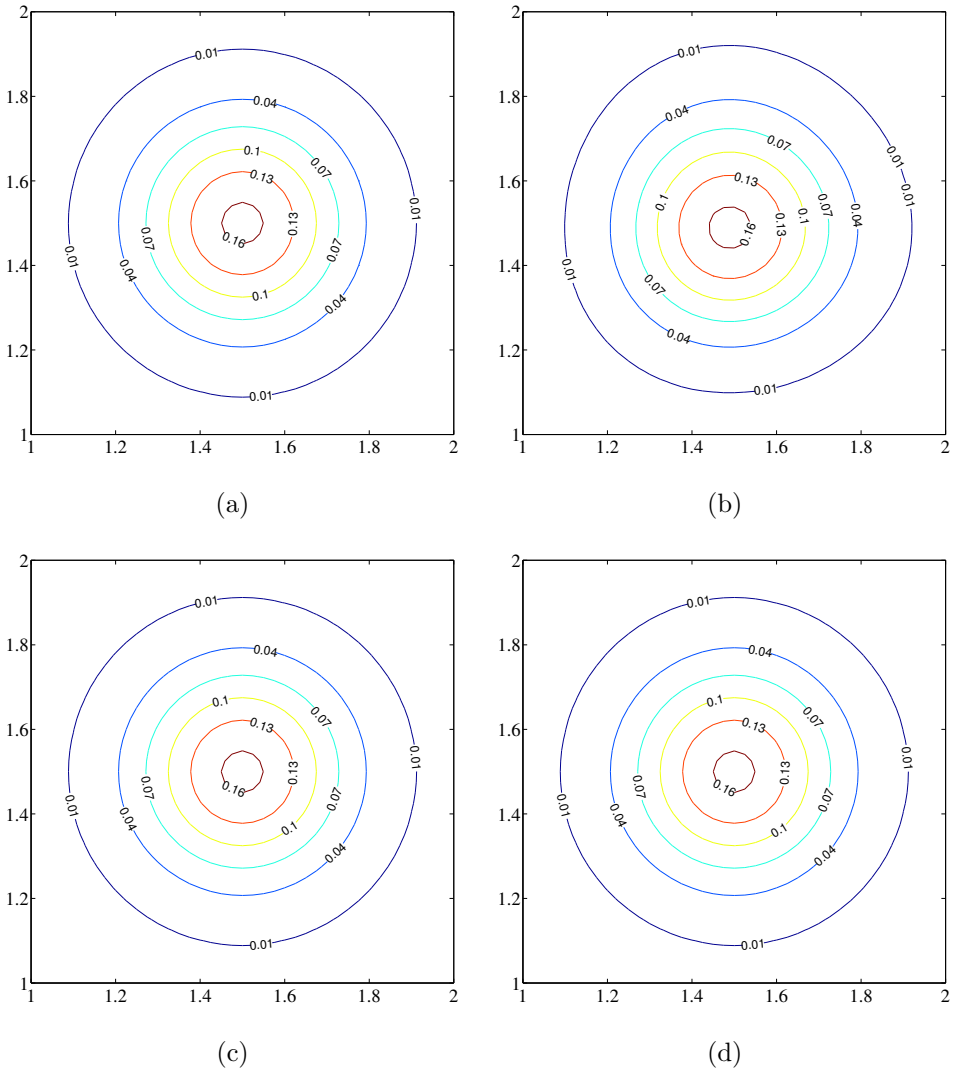

Figure 10: Unsteady convection-diffusion equation, 81×81, $\Delta t = 0.00625$: Contour plots of the pulse in the sub-region $1 \leq x, y \leq 2$ at $t = 1.25$ by the analytic solution (a), standard PR-ADI (b), ADI-CIRBF-1 (c) and ADI-CIRBF-2 (d).

successive time levels is small, *i.e.* less than a given tolerance, the obtained solution is the solution to (4).

In the present calculation, we employ a set of uniform grids $\{11\times 11, 16\times 16, \ldots, 51\times 51\}$ and a time step of 0.0005. Figure 11 displays the solution accuracy against the grid size, which shows the superiority of the two present schemes over the standard PR-ADI scheme. The solution converges apparently as $O(h^{1.94})$, $O(h^{3.02})$ and $O(h^{4.53})$ for PR-ADI, ADI-CIRBF-1 and ADI-CIRBF-2, respectively. Additionally, Figure 12 show that profiles of u along the centrelines by ADI-CIRBF-1 and ADI-CIRBF-2 agree very well with the analytic solutions.

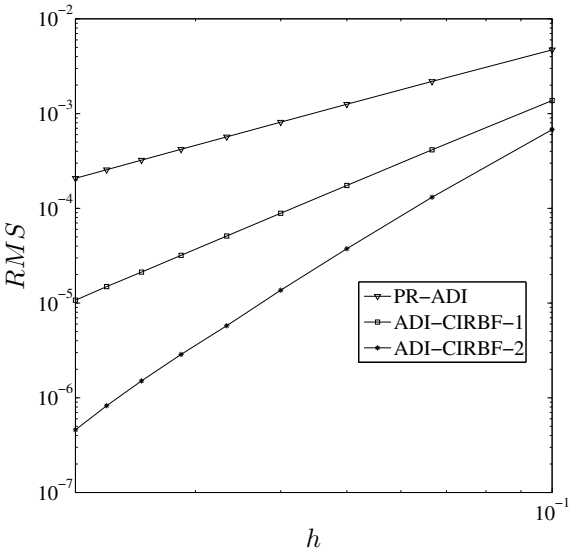

Figure 11: Steady convection-diffusion equation, $\{11\times 11, 16\times 16, \ldots, 51\times 51\}$: The effect of grid size h on the solution accuracy for the standard PR-ADI and two present schemes. The solution converges as $O(h^{1.94})$, $O(h^{3.02})$ and $O(h^{4.53})$ for PR-ADI, ADI-CIRBF-1 and ADI-CIRBF-2, respectively.

5 Concluding remarks

This paper presents new high-order approximation schemes for the discretisation of convection-diffusion equations in two dimensions. The ADI algorithm is adopted in the form in which the operator is factorised into four separate terms rather than the usual two, while compact integrated-RBFs are implemented to represent the

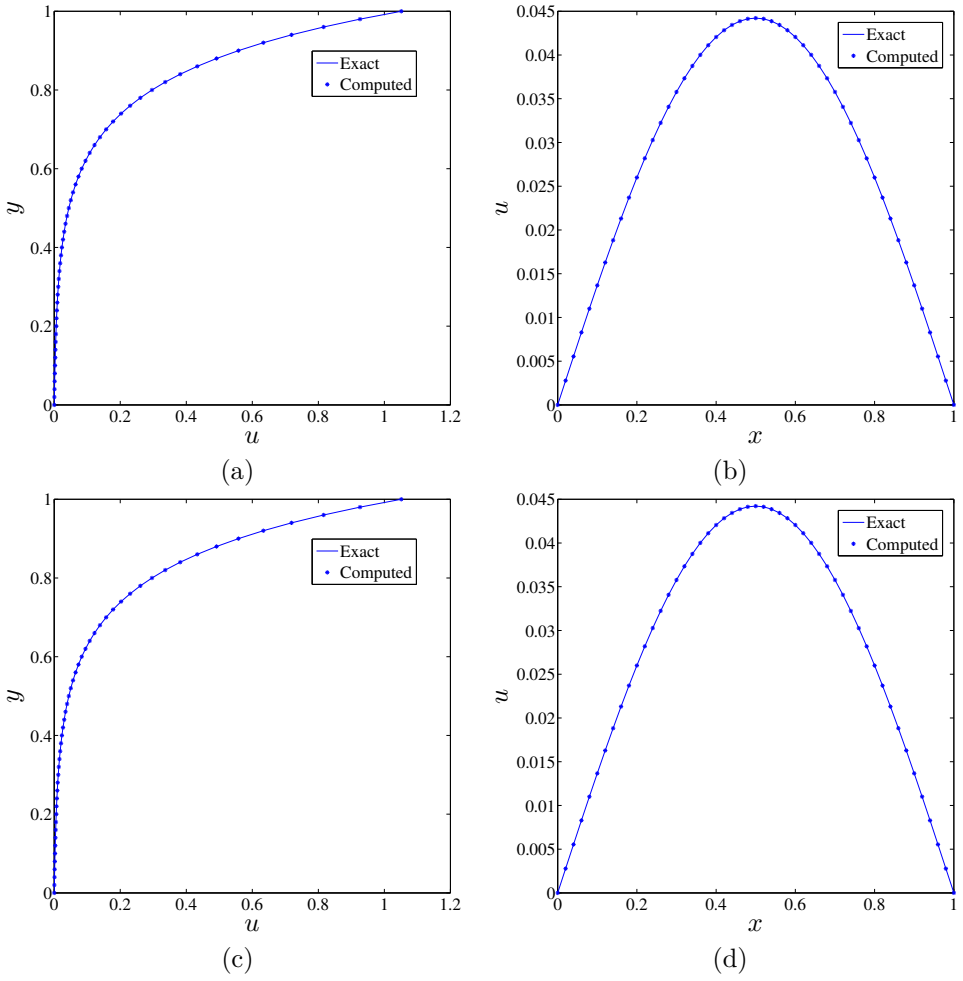

Figure 12: Steady convection-diffusion equation, 51×51: Profiles of the solution u along the vertical and horizontal centrelines by ADI-CIRBF-1 (a)-(b) and ADI-CIRBF-2 (c)-(d).

variable and its derivatives over 3-point stencils. Two CIRBF schemes are proposed, which lead to a significant improvement in accuracy over the central-finite-difference-based ADI method. CIRBF-2 scheme, where first-order and second-order derivatives are approximated separately, is found to be more efficient and effective than CIRBF-1 scheme, where first-order and second-order derivatives are approximated simultaneously. We note that the assumption of rectangular domain

here is not necessary and the present methods can easily treat non-rectangular domains.

Acknowledgement: Thai-Quang would like to thank USQ, FoES and CESRC for a postgraduate research scholarship. This work was supported by the Australian Research Council.

References

Crank, J.; Nicolson, P. (1996): A practical method for numerical evaluation of solutions of partial differential equations of the heat-conduction type. *Advances in Computational Mathematics*, vol. 6, no. 1, pp. 207–226.

Dehghan, M. (2004): Weighted finite difference techniques for the one-dimensional advection-diffusion equation. *Applied Mathematics and Computation*, vol. 147, no. 2, pp. 307–319.

Douglas, J.; Rachford, H. (1956): On the numerical solution of heat conduction problems in two and three space variables. *Transactions of the American mathematical Society*, vol. 82, no. 2, pp. 421–439.

Franke, R. (1982): Scattered data interpolation: Tests of some method. *Mathematics of Computation*, vol. 38, pp. 181–200.

Glowinski, R.; Ciarlet, P. G.; Lions, J. L. (2003): *Numerical methods for fluids*. Elsevier Science & Technology.

Isenberg, J.; Gutfinger, C. (1972): Heat transfer to a draining film. *International Journal of Heat and Mass Transfer*, vol. 16, no. 2, pp. 505–512.

Kalita, J. C.; Chhabra, P. (2006): An improved (9,5) higher order compact scheme for the transient two-dimensional convection-diffusion equation. *International Journal for Numerical Methods in Fluids*, vol. 51, no. 7, pp. 703–717.

Kalita, J. C.; Dalal, D. C.; Dass, A. K. (2002): A class of higher order compact schemes for the unsteady two-dimensional convection-diffusion equation with variable convection coefficients. *International Journal for Numerical Methods in Fluids*, vol. 38, no. 12, pp. 1111–1131.

Karaa, S.; Zhang, J. (2004): High order adi method for solving unsteady convection-diffusion problems. *Journal of Computational Physics*, vol. 198, no. 1, pp. 1–9.

Ma, Y.; Sun, C.-P.; Haake, D. A.; Churchill, B. M.; Ho, C.-M. (2012): A high-order alternating direction implicit method for the unsteady convection-dominated diffusion problem. *International Journal for Numerical Methods in Fluids*, vol. 70, no. 6, pp. 703–712.

Mai-Duy, N.; Tran-Cong, T. (2008): Integrated radial-basis-function networks for computing newtonian and non-newtonian fluid flows. *Computers & Structures*, vol. 87, no. 11-12, pp. 642–650.

Noye, B. J.; Tan, H. H. (1989): Finite difference methods for solving the two-dimensional advection-diffusion equation. *International Journal for Numerical Methods in Fluids*, vol. 9, no. 1, pp. 75–98.

Parlange, J. Y. (1980): Water transport in soils. *Annual Review of Fluid Mechanics*, vol. 12, no. 1, pp. 77–102.

Peaceman, D. W.; H. H. Rachford, J. (1955): The numerical solution of parabolic and elliptic differential equations. *Journal of the Society for Industrial and Applied Mathematics*, vol. 3, no. 1, pp. 28–41.

Sheu, T. W. H.; Kao, N. S. C.; Chiu, P. H.; Lin, C. S. (2011): Development of an upwinding scheme through the minimization of modified wavenumber error for the incompressible navier-stokes equations. *Numerical Heat Transfer, Part B: Fundamentals*, vol. 60, no. 3, pp. 179–202.

Thai-Quang, N.; Le-Cao, K.; Mai-Duy, N.; Tran-Cong, T. (2012): A high-order compact local integrated-rbf scheme for steady-state incompressible viscous flows in the primitive variables. *CMES: Computer Modeling in Engineering & Sciences*, vol. 84, no. 6, pp. 528–558.

Thomas, J. W. (1995): *Numerical Partial Differential Equations: Finite Difference Methods*. Springer, New York.

Tian, Z. F.; Ge, Y. B. (2007): A fourth-order compact adi method for solving two-dimensional unsteady convection-diffusion problems. *Journal of Computational and Applied Mathematics*, vol. 198, no. 1, pp. 268–286.

You, D. (2006): A high-order padé adi method for unsteady convection-diffusion equations. *Journal of Computational Physics*, vol. 214, no. 1, pp. 1–11.